Modeling Source/Drain Contact Resistance in Nanoscale MOSFETs

E. Chen*, Anson C-C Wang, H.S. Chen, W.H. Hsieh, T-H Yu, T.M. Shen, Jeff Wu, and C.H. Diaz
TCAD Division, Taiwan Semiconductor Manufacturing Company (TSMC)
No. 168, Park Ave. 2, Hsinchu Science Park, Hsinchu County, Taiwan
E-mail*: chenjhm@tsmc.com

***Abstract*—The influence of S/D contact resistance (R_{csd}) on MOSFETs performance becomes increasingly significant with aggressive scaling. However, the highly non-uniform doping and the presence of non-silicon element(s), such as $Si_{1-x}Ge_x$ for *p*-MOSFET, render the existing TCAD model inadequate for the purpose of design and optimization of the S/D contact regions. In this study, compact R_{csd} models for both *n*- and *p*-MOSFETs are developed to capture the doping and germanium mole fraction dependence. Both models are validated with experimental results, while the *n*-MOSFET model is also successfully used in full flow simulations with excellent agreements to silicon experimental data, correctly reflecting the S/D doping dependence of *ON*-current (I_{dsat}) and threshold voltage (V_{tsat}).**

Keywords-S/D contact resistance, nanoscale MOSFET, $Si_{1-x}Ge_x$ S/D, doping-dependent, and germanium mole fraction dependent

I. INTRODUCTION

The influence of source/drain (S/D) contact resistance (R_{csd}) on the performance of metal-oxide-semiconductor field-effect transistors (MOSFETs) becomes increasingly significant with aggressive scaling. In nanoscale MOSFETs, both the channel and S/D parasitic resistance show significant influence on the device performance. Thus, an accurate model for *n*- and *p*- type R_{csd}'s is essential for designing and optimizing the S/D contact regions. However, the existing TCAD model becomes inadequate for this purpose due to the much increased complexity of the S/D structure of nanoscale MOSFETs. For *n*-MOSFETs, the S/D contact silicide is not only adjacent to the S/D contact area, but also to the S/D extension (SDE). The ultra-shallow junctions of the SDE lead to highly non-uniform doping concentrations around the silicide region. In addition, $Si_{1-x}Ge_x$ raised S/D for the performance enhancement of *p*-MOSFET [1] presents non-silicon elements in the S/D regions and makes it necessary to re-model *p*-MOSFET R_{csd} as germanium mole fraction dependent. In this study, compact R_{csd} models for both *n*- and *p*-MOSFETs are developed to capture the doping and germanium mole fraction dependence. Both models are validated with experimental results. Moreover, the *n*-MOSFET model is also successfully used in full flow simulations with excellent agreements to silicon experimental data, correctly reflecting the S/D doping dependence of *ON*-current (I_{dsat}) and threshold voltage (V_{tsat}).

II. MODEL DEVELOPMENT AND VALIDATAION

Firstly, the R_{csd} is defined as the reciprocal of the derivative of current density with respect to voltage at zero bias [2]

$$R_{csd} \equiv \left(\frac{\partial J}{\partial V}\right)^{-1}_{V=0}. \qquad (1)$$

For metal-semiconductor contact, the current density includes both thermionic and tunneling components. In practice, the doping concentration of SDE in nanoscale MOSFETs is still larger than 10^{19} cm^{-3}, the current density is dominated by tunneling process. Therefore, R_{csd} can be given by [3]

$$R_{csd} = R_{\infty}\frac{300\mathrm{K}}{T}\exp\left(\frac{q\Phi_{\mathrm{Bn}}}{\mathrm{E}_0}\right), \qquad (2)$$

where R_{∞} is the Schottky resistance as the doping concentration approaches infinity or Schottky barrier height approaches zero, T is the lattice temperature, and

$$\mathrm{E}_0 = \mathrm{E}_{00}\coth\left(\frac{\mathrm{E}_{00}}{k_B T}\right). \qquad (3)$$

In Eq.(3), E_{00} is an energy given by

$$\mathrm{E}_{00} = \frac{q\hbar}{2}\sqrt{\frac{\left|N_{D,0} - N_{A,0}\right|}{\varepsilon_s m_t}}, \qquad (4)$$

where $\left|N_{D,0} - N_{A,0}\right|$ is the S/D net doping concentration around silicide contact, ε_s is the semiconductor permittivity, and m_t is the tunneling mass.

A. n-MOSFETs

For *n*-MOSFETs, the most commonly used nickel silicide (NiSi) is considered as the contact metal. Fig.1 shows the energy-band diagram incorporating Schottky effect for metal *n*-type silicon at thermal equilibrium. The intrinsic barrier height of NiSi is Φ_{Bn0} = 0.66 eV [4], and the effective barrier height Φ_{Bn} is lowered due to the combined effects of the field and the image force. The right-hand side of the figure shows the six degenerate states at the conduction band edge of silicon. In principle, the total tunneling current should include the tunneling contributions from all six degenerate states at the conduction band edge. Nevertheless, the two degenerate states with the longitudinal effective mass as the tunneling mass have a much lower tunneling probability than the rest of states with the transverse effective mass, when (100) Si is considered. Therefore, the tunneling mass can be approximated as the transverse effective mass ($m_t = 0.19m_0$).

 ISBN 978-0-615-71756-2

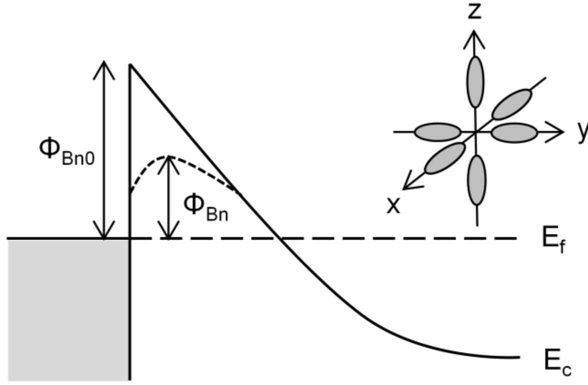

Fig.1 Energy-band diagram incorporating Schottky effect for metal *n*-type silicon at thermal equilibrium. The intrinsic barrier height is Φ_{Bn0}. The effective barrier height is lowered as Φ_{Bn} due to the combined effects of the field and the image force. The right-hand side shows the six degenerate states at the conduction band edge of silicon.

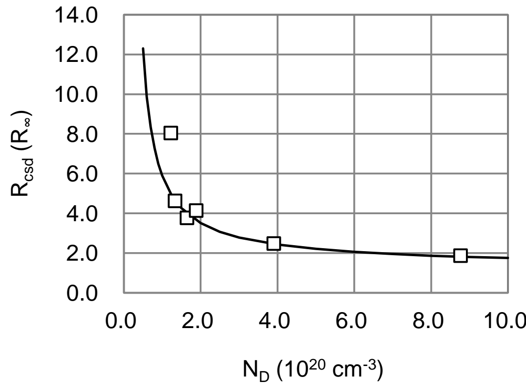

Fig.2 *n*-MOSFET R_{csd} model (solid line) and experimental result (empty squares).

Using the tunneling mass and two fitting parameters: $R_\infty = 10^{-8} \sim 10^{-9}$ Ω-cm^2 and $\Phi_{Bn} = 0.22$ eV, Fig.2 shows the experimental results (empty squares) and the model calculation (solid line). The first fitting number reflects the resistance limit of the NiSi/Si Schottky junction. The second one can be estimated from the barrier lowering formula,

$$\Delta\Phi = \sqrt{\frac{qF_m}{4\pi\varepsilon_s}}, \tag{5}$$

where F_m is the maximum field at the interface. If the *n*-type doping concentration of 8×10^{20} cm^{-3} is around the S/D contact regions, Eq.(5) gives 0.43 eV of barrier lowering, which results in 0.23 eV of Φ_{Bn}. It can be seen that the analytical estimation is quite close to the experimental extraction. Because barrier lowering dominates the current density at high doping concentration, the benefit of further increase of S/D doping concentration diminishes. Fig.2 shows the R_{csd} reduction starts to saturate as the S/D doipng concentration goes beyond 4×10^{20} cm^{-3}.

B. p-MOSFETs

For *p*-MOSFET, the S/D areas are replaced by $Si_{1-x}Ge_x$ material due to the advantage of channel mobility. In the real case, S/D $Si_{1-x}Ge_x$ may lie in between relaxed and compressively strained conditions. In this model, the bandstructure of fully strained $Si_{1-x}Ge_x$ on (100) Si is considered. This is a good approximation due to the small difference between the dominant masses for both relaxed and strained conditions [5]. It is noted that the constant energy spheres of the light-hole (LH) and heavy-hole (HH) of $Si_{1-x}Ge_x$ material are highly anisotropic. For the compact model purpose, the density-of-state (DOS) effective masses are used to capture the average contribution from the different tunneling directions. Fig.3 shows the DOS effective masses of the holes for the condition of $Si_{1-x}Ge_x$ on Si (100). As the germanium mole fraction increases, both masses decreases, which leads larger tunneling probability than pure silicon.

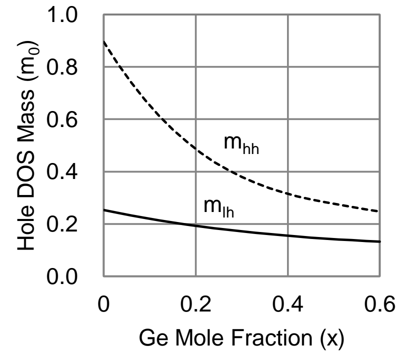

Fig.3 Hole DOS mass vs. germanium mole fraction for the condition of $Si_{1-x}Ge_x$ on Si (100).

Since the tunneling probability has an exponential dependence on the effective mass, LH band dominates the tunneling current due to the lower effective mass as shown in Fig.3. The tunneling mass, $m_t(x)$, is approximated by the LH DOS effective mass (for $x < 0.8$), [6]

$$m_t(x) = m_{lh}(x) = \left(-0.1432x^3 + 0.3618x^2 - 0.3669x + 0.2534\right)m_0 . \tag{6}$$

As the germanium mole fraction increases, the HH band starts to contribute the tunneling current. In order to consider the current contribution, R_∞ is modified empirically and given by (for $x < 0.8$),

$$R_\infty' = R_\infty(1-x)^2 . \tag{7}$$

The last parameter, Φ_{Bp}, is set at 0.22 eV similar to *n*-MOSFET's. The reason is that the barrier height of transition metal silicide is usually at mid-gap due to the Fermi level pinning by the surface states. Although the valence band energy shifts as germanium mole fraction increases, the same

barrier heights are assumed for both *n*- and *p*- contacts. Using the above parameters, Fig.4 shows *p*-MOSFET R_{csd} model (solid line) and experimental results (empty squares) when $N_a = 3\times10^{20}$ cm^{-3}. The model predictions agree well with the experimental results under various germanium mole fractions. It is noted that employing $Si_{1-x}Ge_x$ S/D not only improves the channel mobility, but also reduces the contact resistance. As shown in Fig.4, when using a 40%Ge S/D, R_{csd} is almost 1/3 of silicon S/D case. Adding germanium to S/D region is more effective in reducing contact resistance than increasing S/D doping concentration. In addition to the germanium dependence, Fig.5 shows good model (solid line) to experimental results (empty squares) agreement for different doping concentrations when the germanium mole fraction is held at 50%. Similar to the *n*-MOSFET part, increasing doping concentration does not bring much benefit for reducing *p*-MOSFET R_{csd} when acceptor concentration is higher than 3×10^{20} cm^{-3}.

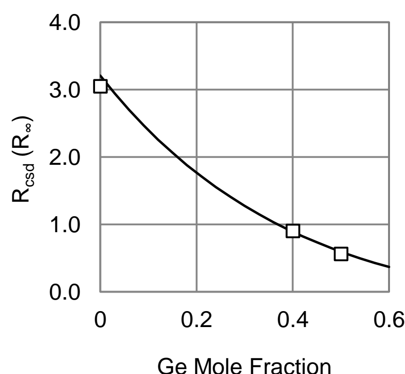

Fig.4 *p*-MOSFET R_{csd} model (solid line) and experimental results (empty squares) show a good agreement under various germanium mole fractions when $N_a = 3\times10^{20}$ cm^{-3}.

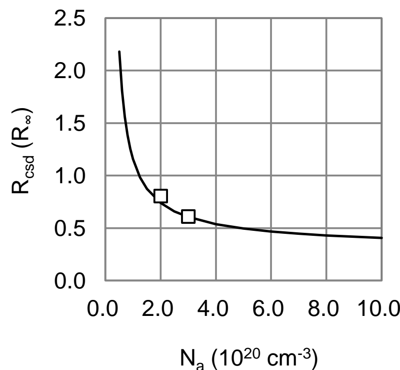

Fig.5 *p*-MOSFET R_{csd} model (solid line) and experimental results (empty squares) show a good agreement for the different doping concentration when the germanium mole fraction of $Si_{1-x}Ge_x$ is held at 50%.

It can be concluded that reducing the tunneling mass is the most effective strategy to reduce R_{csd}. In the case of *n*-MOSFET, it is difficult to achieve much lower tunneling mass by increasing stress because the band warping nearly cancels out each other between six conduction band valleys on the principal axes. Consequently, the typically observed *n*-MOSFET R_{csd} is limited to around twice R_∞ consistent with the model.

III. Full Process and Device Simulation

Finally, a full process and device simulation of the state-of-the-arts *n*-MOSFET is used to further validate the model. Fig.6 shows the schematic cross section reflecting various series resistances [7]: R_{ov} is the accumulation-layer resistance in the gate-source (or -drain) overlap region where the current mainly stays near the surface; R_{ldd} is the resistance in the SDE region; R_{sp} is associated with current spreading from the S/D contact region into SDE region; R_{nisi} is the metal resistance of NiSi material; and R_{plug} is the contact plug resistance. Since the resistivity of NiSi is very low (ρ_{nisi} ~ 10 μΩ-cm), R_{nisi} is neglected in the simulation.

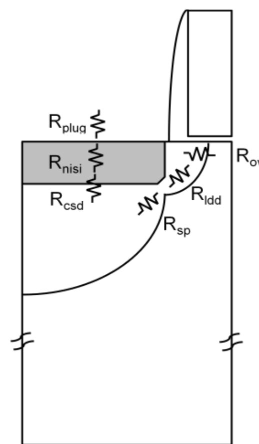

Fig.6 The schematic cross section shows the various contributions to the series resistance in a nanoscale MOSFET. Actually R_{nisi} is negligible due to the low resistivity (ρ_{nisi} ~ 10 μΩ-cm).

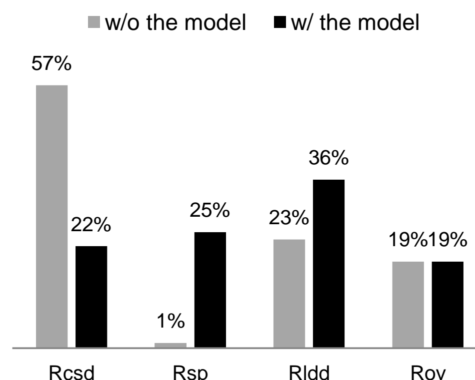

Fig.7 The contribution of various series resistance with and without including the R_{csd} model show the totally different results in the full *n*-MOSFET simulation.

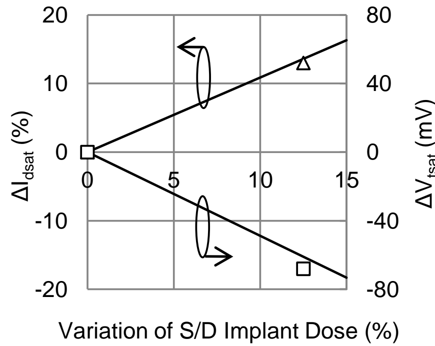

Fig.8 ΔI_{dsat} and ΔV_{tsat} versus the variation of S/D implant dose. The model results (solid line) and the experimental data (symbol) show excellent agreements.

The extracted resistance components by the existing TCAD model, and by the model developed in this paper, are compared in Fig.7. Although both methods show the same magnitude of saturation current (I_{dsat}), the contribution spectrums are very different. It can be seen that the extracted R_{sp} is largely underestimated by the existing model. As a result, the primary tasks suggested by the two models are totally different. The existing model suggests reducing R_{csd} for the future work since it is the largest portion of parasitic resistance. On the contrary, the new model suggests SDE optimization is the most important task to improve the device performance because R_{ldd} is the largest one. Evidently, the result shows that the existing model can lead to incorrect process guidance and non-optimal design. Furthermore, simulation results using our model are compared to silicon experiments with different S/D doses. The excellent agreements of the ΔI_{dsat} and ΔV_{tsat} to silicon data are clearly shown in Fig.8.

I. CONCLUSION

In conclusion, the S/D contact resistance in nanoscale MOSFETs has been successfully modeled in the study. The doping-dependent *n*- and *p*-MOSFET R_{csd}'s are dominated by barrier lowering. Because of the smaller tunneling mass in $Si_{1-x}Ge_x$ on (100) Si, the *p*-MOSFET R_{csd} keeps decreasing as the germanium mole fraction increases. The model would be instrumental for optimization of S/D structures in the future development of nanoscale MOSFETs.

REFERENCES

[1] M.C. Öztürk ,J. Liu, H. Mo, and N. Pesovic, "Advanced $Si_{1-x}Ge_x$ source/drain and contact technologies for sub-70 nm CMOS," in *IEDM Tech. Dig.*, pp. 375-378, 2002.

[2] S.M. Sze, "Physics of semiconductor devices," John Siley & Sons, Inc., 1981.

[3] F.A. Padovani and R. Stratton, "Field and thermionic-field emission in Schottky barriers," Solid-State Electron., vol. 9, pp. 695-707, 1966.

[4] G. Ottaviani, K.N. Tu, and J.W. Mayer, "Barrier heights and silicide formation for Ni, Pd, and Pt on silicon," Phys. Rev. B, vol. 24, pp. 3354-3359, 1981.

[5] M.V. Fischetti and S.E. Laux, "Band structure, deformation potentials, and carrier mobility in strained Si, Ge, and SiGe alloys," J. Appl. Phys., vol. 80, pp. 2234-2252, 1996.

[6] L. Yang, J.R. Waltling, R.C.W. Wilkins, M. Boriçi, J.R. Barker, A. Asenov, and S. Roy, "Si/SiGe heterostructure parameters for device simulations," Semicond. Sci. Technol., vol. 19, pp. 1174-1182, 2004.

[7] Y. Taur and T.H. Ning, "Fundamentals of modern VLSI devices," Cambridge University Press, 1998.